

Laue Lens Development for Hard X-rays (>60 keV)

D. Pellicciotta, F. Frontera, G. Loffredo, A. Pisa, K. Andersen, P. Courtois, B. Hamelin, V. Carassiti, M. Melchiorri, S. Squerzanti

Abstract—Results of reflectivity measurements of mosaic crystal samples of Cu (111) are reported. These tests were performed in the context of a feasibility study of a hard X-ray focusing telescope for space astronomy with energy passband from 60 to 600 keV. The technique envisaged is that of using mosaic crystals in transmission configuration that diffract X-rays for Bragg diffraction (Laue lens). The Laue lens assumed has a spherical shape with focal length f . It is made of flat mosaic crystal tiles suitably positioned in the lens. The samples were grown and worked for this project at the Institute Laue-Langevin (ILL) in Grenoble (France), while the reflectivity tests were performed at the X-ray facility of the Physics Department of the University of Ferrara.

Index Terms—X-ray, Astronomy, Telescope, Bragg, Laue, Crystals.

I. INTRODUCTION

THE role of hard X-ray astronomy (>10 keV) is now widely recognized. A breakthrough in the sensitivity of the hard X-ray telescopes, which today are based on detectors that view the sky through (or not) coded masks (e.g., [1], [2]), is expected when focusing optics will be available also in this energy range. Focusing techniques are now in an advanced stage of development. The best technique to focus hard X-rays with energy less than about 70 keV, appears to be Bragg diffraction from multilayers. These are made of a set of bilayers, each consisting of a low Z together with a high Z material, with graded thickness (see e.g. [3]). Above 70 keV, multilayer mirrors become inefficient (e.g. [4]) and Bragg diffraction from mosaic crystals in transmission configuration (Laue geometry) appears to be the most efficient way to face the focusing problem at these energies. Mosaic crystals and their diffraction properties have been known for many years; for a reference book see [5]. By mosaic crystal we mean a crystal made of microscopic perfect crystals (crystallites), with their lattice planes slightly misaligned with each other around a mean direction according to a distribution function which

can be approximated by a Gaussian:

$$W(\Delta) = \frac{1}{\sqrt{2\pi}\eta} \exp\left(-\frac{\Delta^2}{2\eta^2}\right) \quad (1)$$

where Δ is the magnitude of the angular deviation of the crystallites from the mean direction, and η is the standard deviation of the distribution. The Full Width at Half Maximum (FWHM) of the Gaussian function defines the mosaic spread $\beta \approx 2.35\eta$ of the mosaic crystal.

In general, the X-rays which impinge on a perfect crystal are diffracted according to the Bragg law:

$$2d \sin \theta_B = n \frac{hc}{E} \quad (2)$$

where θ_B (Bragg angle) is the angle between the lattice planes and the direction of both the incident and diffracted photons, $2\theta_B$ is known as diffraction angle, d (in Å) is the distance between lattice planes, n ($= 1, 2, \dots$) is the diffraction order,

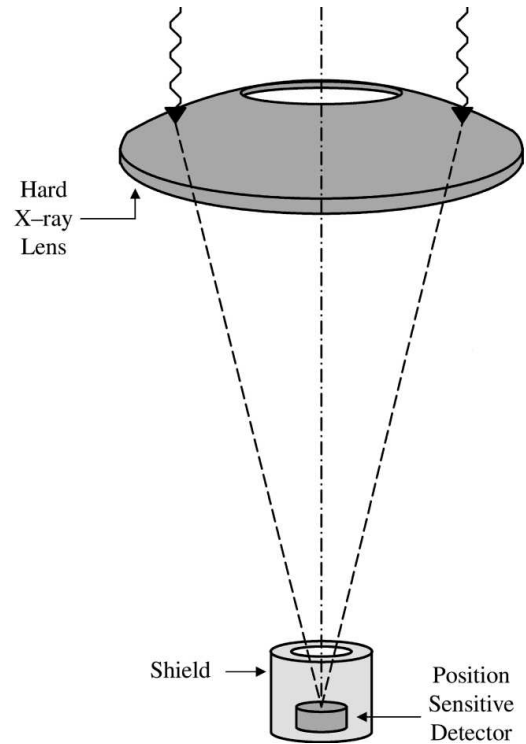


Fig. 1. Pictorial view of a Laue lens (not to scale). The lens is made of mosaic crystal tiles in transmission configuration. The impinging photons are diffracted by the crystal tiles and focused in a small region centred in the focus of the lens where a position-sensitive detector is positioned.

D. Pellicciotta is with Physics Dept, University of Ferrara, Ferrara, Italy.

F. Frontera is with Physics Dept, University of Ferrara, Ferrara, Italy and with IASF, CNR, Bologna, Italy.

G. Loffredo is with Physics Dept, University of Ferrara, Ferrara, Italy.

A. Pisa is with Physics Dept, University of Ferrara, Ferrara, Italy.

K. Andersen is with Institute Laue-Langevin, Grenoble, France.

P. Courtois is with Institute Laue-Langevin, Grenoble, France.

B. Hamelin is with Institute Laue-Langevin, Grenoble, France.

V. Carassiti is with INFN, Ferrara, Italy.

M. Melchiorri is with INFN, Ferrara, Italy.

S. Squerzanti is with INFN, Ferrara, Italy.

E (in keV) is the photon energy and $hc = 12.4 \text{ keV}\cdot\text{\AA}$. In the case of a mosaic crystal, thanks to its mosaic β , when a polychromatic parallel beam of X-rays impinges on it with mean Bragg angle θ_B , photons in a bandwidth

$$\Delta E = E \beta / \tan \theta_B \quad (3)$$

are diffracted by the crystal.

The goal of our project is to develop a broad band hard X-/gamma-ray ($>60 \text{ keV}$) focusing telescope devoted to the study of the continuum emission from celestial sources. The technique envisaged is that of using mosaic crystals in transmission configuration and the telescope is designed to be made of mosaic crystal tiles (Laue lens), where the reflected X-ray beam emerges from the surface opposite to the crystal front surface. Laue lenses devoted to the study of the gamma-ray emission from nuclear lines, and thus with a relatively narrow energy passband, have been already developed and tested (see, e.g., [6], [7]).

II. SUMMARY OF THE LENS MAIN PROPERTIES

Results of the feasibility study of our lens have already been reported [8]. Here we summarize the most relevant results.

The lens of our project has a spherical shape (see Fig. 1) with radius R and focal length $f = R/2$. In the lens focus a detector is positioned. The detector is required to have a high detection efficiency in the lens passband (see below) and a position sensitivity proportioned to the imaging capabilities of the lens.

The crystal tiles are assumed to have their lattice planes perpendicular to their front surfaces (see Fig. 2), to be flat and with small square cross section ($\sim 1 \times 1 \text{ cm}^2$) in order to best approximate the spherical profile.

Consistent with the Bragg diffraction principles above summarized, the photons in a band ΔE around a given energy E which impinge on the lens parallel to the instrument axis (z axis in Fig. 2) are diffracted only by those crystals which have their lattice planes oriented in such a way as to satisfy Eq. 3, where θ_B is the average Bragg angle (see Eq. 2) of these crystals (see also Fig. 2). Photons with the centroid energy E are diffracted from their initial direction (see Fig. 2) by an angle $2\theta_B$, and are focused at point O of the focal plane if they impinge on the center of the crystal tile front surface, as in Fig. 2.

The lens external diameter increases with f , while its surface approximately increases with f^2 .

The mosaic crystal tiles are disposed in the lens according to an Archimedes' spiral (see Fig. 10). Thanks to this disposition the centroid energy of the bandwidth ΔE (Eq. 3) changes in a very smooth manner along the spiral. Fig. 3 shows the reflectivity profiles of 3 contiguous crystals along the spiral curve. As a consequence of the Archimedes' spiral disposition, the effective area of the lens, defined as the lens geometric area projected in the focal plane times the mean reflection efficiency, smoothly changes with energy, apart from jumps due to the contribution from higher diffraction orders (see Fig. 11).

The nominal energy passband of the Laue lens (E_{min}, E_{max}) is related to the range of diffraction angles

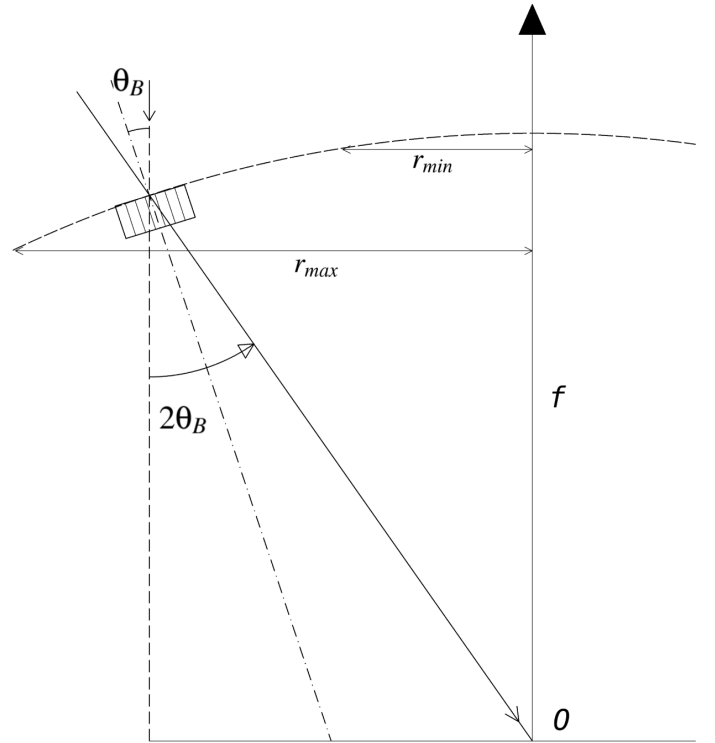


Fig. 2. Scheme of the Bragg diffraction in a Laue lens. The X-ray photons in a given energy band ΔE around E , which impinge on the lens parallel to the z axis (lens axis), are diffracted only by those mosaic crystals oriented in such a way as to satisfy Eq. 3. The photons with centroid energy E which hit the center of these crystals are focused in the lens focus (point O), r_{max} and r_{min} define the innermost and outermost radius of the lens surface, respectively.

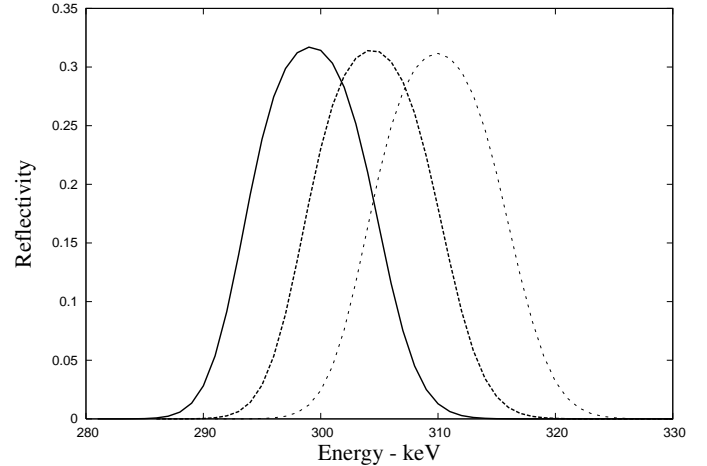


Fig. 3. An example of the reflectivity profile of three contiguous crystals along an Archimedes' spiral.

($\theta_{max}, \theta_{min}$) that are covered by the lens due to its spherical geometry, and thus (see Fig. 2) to the outer and inner radii r_{max} and r_{min} of the spherical segment. From the Bragg law, with simple calculations, it can be shown that

$$E_{min} = \frac{hc}{2d \sin \theta_{max}} \approx \frac{hc f}{d r_{max}} \quad (4)$$

$$E_{max} = \frac{hc}{2d \sin \theta_{min}} \approx \frac{hcf}{d r_{min}}. \quad (5)$$

III. MOSAIC CRYSTAL CHOICE AND SAMPLE TEST RESULTS

The reflection efficiency of the mosaic crystals, according to the theoretical model by [5], is given by the following equation:

$$R(\Delta, E) = \frac{I_d(\Delta, E)}{I_0} = \frac{1}{2}(1 - e^{-2\sigma T})e^{-\mu \frac{T}{\gamma_0}} \quad (6)$$

where I_0 is the intensity of the incident beam, $I_d(\Delta, E)$ is the intensity of the diffracted beam, μ is the absorption coefficient per unit length at energy E , γ_0 is the cosine of the angle between the direction of the photons and the normal to the crystal surface, T is the thickness of the mosaic crystal, and σ is given by:

$$\sigma = \sigma(E, \Delta) = W(\Delta)Q(E) \quad (7)$$

where

$$Q(E) = \left| \frac{r_e F}{V} \right|^2 \lambda^3 \frac{1 + \cos^2(2\theta_B)}{2 \sin 2\theta_B} \quad (8)$$

in which $r_e (= 2.815 \times 10^{-5} \text{Å})$ is the classical electron radius, F is the structure factor, V is the volume of the crystal unit cell, λ is the photon wavelength corresponding to the energy E , and θ_B is the Bragg angle.

As can be seen from Eq. 6, the mosaic reflectivity depends on various parameters, including the crystal material and the mosaic spread. As a result of our feasibility study [8], we have determined, in addition to the best lens shape and disposition of the crystals in the lens as discussed above, the best candidate materials and their required mosaic properties for photons in the energy range of interest.

Unfortunately the technological development of mosaic crystals is still in its infancy and only a few materials are available in a mosaic structure with the desired properties. Fortunately, for one of the best candidate materials (Copper), the technology has been recently developed at the Institute Laue-Langevin (ILL) in Grenoble (France).

In order to test the quality of the produced material and its compatibility with the Laue lens constraints, some samples of Cu (111) of different thickness and mosaic spread, with their lattice planes perpendicular to the crystal front surfaces, have been tested, and the reflectivity results compared with the expectations of the mosaic crystal diffraction theory (Eq. 6).

We concentrated our measurements on crystal samples with thickness in the 2-4 mm range, which is optimum for our lens (upper energy threshold of 600 keV), and with a mosaic spread below 6 arcmin. This upper limit is the maximum acceptable for low focal lengths (a few meters), given that the spread affects the focal spot size, which increases with the focal length and affects the telescope sensitivity through the focal plane detector background under the spot.

The picture of the front surface of one of these samples is shown in Fig. 4. The tests were performed at the X-ray facility of the Physics Department of the University of Ferrara. The Ferrara X-ray facility (see Fig. 5) allows the use of either polychromatic or monochromatic X-ray beams

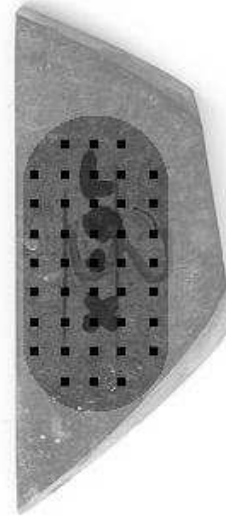


Fig. 4. Picture of the front surface of a 2.5 mm thick crystal sample of Cu (111), that was tested with a pencil beam of polychromatic photons with $1.2 \times 1 \text{ mm}^2$ cross section. The grid of the crystal surface positions hit by the beam is shown. Lattice planes are perpendicular to the front surface and parallel to the grid columns (vertical). The shady structures in the middle of the crystal are superficial inscriptions.

in the energy range from about 10 keV to 140 keV. This facility is currently used for various types of measurements, from the calibration or test of hard X-ray detectors to the test of hard X-ray mirrors. A description of the facility for the calibration of the JEM-X experiment ([9]) aboard the INTEGRAL gamma-ray astronomy satellite now in orbit, and the project for the expansion of this facility now in progress, can be found elsewhere ([10], [11]).

Using a polychromatic pencil beam of hard X-ray photons with $1 \times 1.2 \text{ mm}^2$ cross section, we measured the reflectivity of



Fig. 5. The X-ray facility of the Physics Department of the University of Ferrara and its main components. On the left side: Ortec HPGe detector; in the center: sample holder; on the right: terminal collimator of the X-ray photon beam.

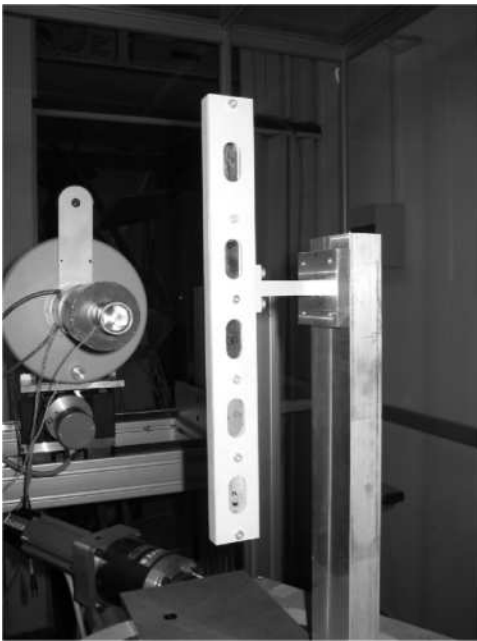


Fig. 6. Holder and crystal samples used for the reflectivity tests.

the samples at a grid of points over the crystal front surface (see Fig. 4). The tested crystals (see Fig. 6) were oriented in order to get a mean Bragg angle θ_B with respect to the polychromatic pencil beam corresponding to an energy of 90-100 keV. The crystal samples could be rotated in order to change, if desired, the energy centroid of diffracted photons (see Eq. 2). The intensity of the direct and diffracted beams were measured with a portable cooled HPGe detector by Ortec (energy resolution better than 1% at 122 keV).

Given the polychromatic nature of the beam, after subtraction of the detector background, the ratio between the diffracted and the direct beam gives the X-ray reflectivity profile of the crystal cross section hit by the photons. The X-ray reflectivity curve at different points of the crystal surface was measured by moving the crystal holder in a plane perpendicular to the pencil beam.

For each sample, two sets of measurements were performed: one set before the removal of a thin layer of material from the crystal surfaces, and the other set after this removal.

All the reflectivity curves were fit with the reflectivity model function of mosaic crystals in a Laue configuration (Eq. 6). We used the CERN code MINUIT to perform the fit to the data. The free parameters of the fit were the Bragg angle, the mosaic spread β and the thickness t_0 of the crystallites. Given that the last parameter was not well constrained, it was fixed at $0.02 \mu\text{m}$.

Fig. 7 is an example of the measured reflectivity curve of a crystal sample of Cu (111) before the removal of the external layer, when the X-ray beam hits the crystal at center of the front surface (see Fig. 4). The best fit model, superposed to the data, is also shown in Fig. 7 along with its best fit parameters. As can be seen, the measured reflectivity profile shows two side wings, which the best fit reflectivity model is unable to describe. Due to these wings, the reflectivity model (Eq. 6)

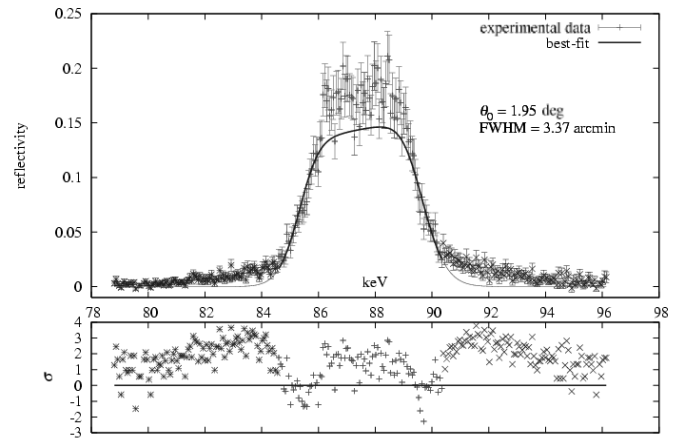


Fig. 7. *Top panel:* Measured reflectivity curve of one of the crystal samples when the pencil beam hits the center of its front surface (see position grid in Fig. 4), before the chemical removal of an external layer. Also shown is the best fit curve obtained by fitting the model function (Eq. 6) to the data. The best fit parameters of the model (Bragg angle of diffraction and FWHM of the mosaic spread) are shown. In the fit, the thickness of the crystallites was frozen ($0.02 \mu\text{m}$). *Bottom panel:* Residuals of the data to the model in units of standard deviations.

is unable to achieve the flat top of the measured profile. This feature is found at all tested points of the crystal surface. For the same crystal sample, Fig. 9(a) shows the distribution of the mosaic spread as a function of the row number of the grid of points tested, for different columns of the grid (see map in Fig. 4).

After the removal of a thin layer of material (0.1 mm) from the crystal, the reflectivity model fits the data significantly better. As an example, in Fig. 8 we show the corresponding reflectivity curve of the same sample of Fig. 7 after the removal

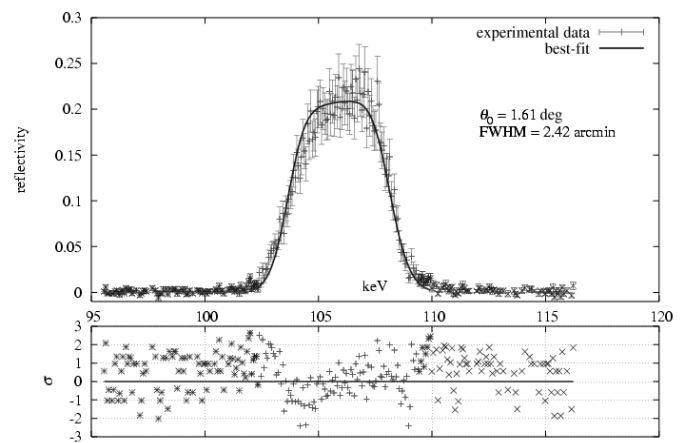
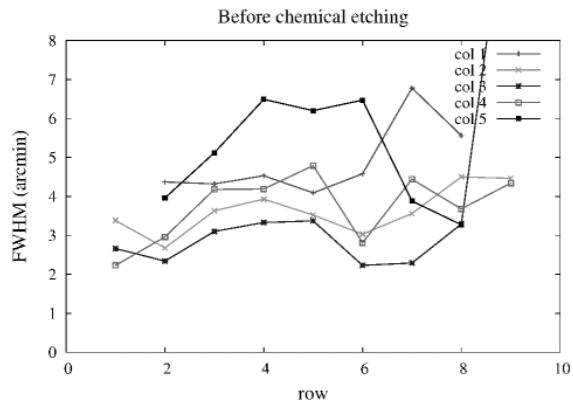
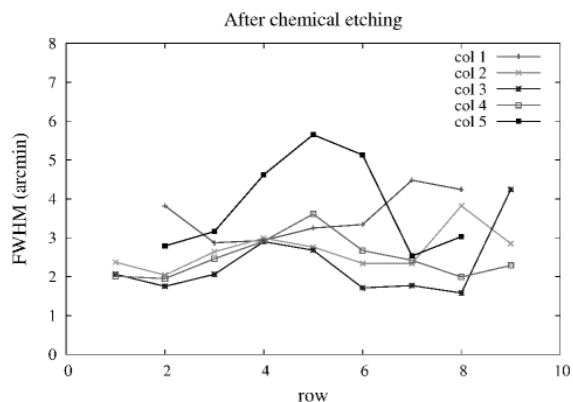


Fig. 8. *Top panel:* Measured reflectivity curve of the same crystal sample of Fig. 7 after the chemical removal of an external layer of 0.1 mm thickness. Also shown is the best fit curve obtained by fitting the reflectivity model function (Eq. 6) to the data. The best fit parameters of the model (Bragg angle of diffraction and FWHM of the mosaic spread) are shown. In the fit, the thickness of the crystallites was frozen ($0.02 \mu\text{m}$). *Bottom panel:* Residuals of the data to the model in units of standard deviations.



(a)



(b)

Fig. 9. Distribution of the measured mosaic spread of the crystal of Fig. 7 as a function of the grid position hit by the pencil beam. *Panel (a)*: before the removal of the external layer of 0.1 mm thickness; *panel (b)*: after the removal of the 0.1 mm thickness.

of the external layer. As can be seen, the side wings are weakened and the reflectivity model well describes the flat top data. These features are repeated at almost any point of the crystal surfaces tested. Fig. 9(b) shows the corresponding distribution of the mosaic spread for the same crystal sample.

A likely explanation for the behaviour of the crystal reflectivity before the removal of the thin layer is that the slicing of the crystal ingot (by means of electro-erosion) to get the samples, perturbs the superficial properties of the crystal tile, giving rise to a reflectivity component with a larger mosaic spread which superposes on that of the crystal bulk. The fact that the fit is still not so good even after the removal of the external layer could also mean that the theory of mosaic crystals is an approximate description of the real crystals. In spite of this, the above results give strong support to our project and open new possibilities for focusing high energy

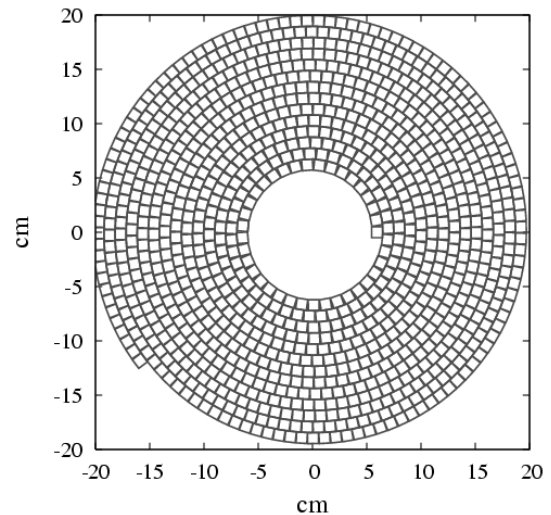


Fig. 10. Configuration of the Laue lens prototype. The crystal tiles are disposed along an Archimedes' spiral (see text).

X-ray photons.

IV. THE LAUE LENS PROTOTYPE

On the basis of the test results obtained, we are developing a Laue lens prototype model (PM) made of 500 Cu (111) crystal tiles (see Fig. 10). The area of the front surface of all crystals is $15 \times 15 \text{ mm}^2$, while the crystal thickness is 2 mm for 415 tiles, and 4 mm for the others. The PM size is shown in Fig. 10, its focal length is 210 cm, and the nominal energy passband is from 60 to 200 keV.

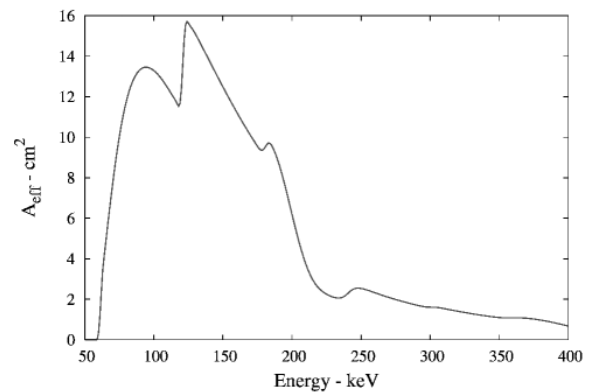


Fig. 11. Expected effective area of the PM as a function of the photon energy, assuming a mosaic spread of 5 arcmin. The nominal energy passband of the PM is from 60 to 200 keV. The jumps in the effective area are due to the higher orders of diffraction from the outermost crystals.

The expected effective area of the PM as a function of the photon energy is shown in Fig. 11, for an assumed mosaic spread of 5 arcmin. As discussed above, the spiral configuration allows a smooth behaviour of the lens effective area with energy, if we exclude the jumps at 120, 180 and 240

keV which are due to the higher orders of diffraction from the outermost crystals.

If the laboratory tests of the prototype are satisfactory, the prototype will also be tested aboard a balloon flight experiment.

V. CONCLUSIONS

We have reported on test results obtained from mosaic crystal samples of Cu (111) produced at the Institute Laue-Langevin of Grenoble (France). According to a theoretical feasibility study of a Laue lens performed by us ([8]), these crystals are among the best materials to be used for maximizing the capabilities of a Laue lens for hard X-rays (> 60 keV) for space astronomy. The sample test results obtained are consistent with the theoretical expectations if a thin external layer is removed from the crystal samples cut from a grown ingot of mosaic crystal of Copper. The mosaic spread of the crystal samples shows a dependence on the crystal surface point hit by the X-ray photons. A better quality control of the crystal production is desirable. These results encouraged us to develop a lens prototype now in progress.

ACKNOWLEDGEMENTS

This research was supported by the Italian Space Agency ASI. We wish to thank John B. Stephen for useful comments and a careful reading of the manuscript.

REFERENCES

- [1] Frontera, F. et al. 1997, *The high energy instrument PDS on-board the BeppoSAX X-ray astronomy satellite*, Astron. & Astrophys. Suppl. Series, Vol. 122, April II 1997, 357-369.
- [2] Ubertini, P. et al. 2003, *IBIS: The Imager on-board INTEGRAL*, Astron. & Astrophys., v. 411, p. L131-L139.
- [3] Joensen, K. D. et al. 1993, *Medium-sized grazing incidence high-energy X-ray telescopes employing continuously graded multilayers*, SPIE Proc., Vol. 1736, p. 239-248.
- [4] Fiore, F. et al. 2004, *HEXIT-SAT: a mission concept for X-ray grazing incidence telescopes from 0.5 to 70 keV*, SPIE Proc., vol. 5488, p. 933-943 (astro-ph/0407647).
- [5] Zachariasen, W. H. 1945, *Theory of X-rays Diffraction in Crystals*, Wiley, New York (USA).
- [6] P. von Ballmoos et al., Proc. 5th INTEGRAL Workshop, Munich 16-20 February, ESA SP-552, 2004.
- [7] H. Halloin et al., *Proc. SPIE*, **5168**, pp. 471-481, 2004.
- [8] Pisa, A. et al. 2004, *Feasibility study of a Laue lens for hard X-rays for space astronomy*, SPIE Proc., vol. 5536, p. 39-48, (astro-ph/0411574).
- [9] Lund, N. et al. 2003, *JEM-X: The X-ray monitor aboard INTEGRAL* Astron. & Astrophys., vol. 411, L231-L328.
- [10] Loffredo, G. et al. 2003, *X-ray facility for the ground calibration of the X-ray monitor JEM-X on board INTEGRAL*, Astron. & Astrophys., vol. 411, L239-L242.
- [11] Loffredo, G. et al. 2005, *The X-ray facility of the Physics Department of the Ferrara University*, Experimental Astronomy, in press.